Stability and Dynamics of Transverse Field Structures in the Optical Parametric Oscillator Near Resonance Detuning

Braxton Osting *
Advisor: Professor Nathan Kutz

June 7, 2005

Abstract

An order parameter equation is derived for an optical parametric oscillator near the resonance detuning limit in two dimensions. The parametric mixing between signal and pump fields with cavity diffraction leads to a quintic, fourth-order evolution equation of the Swift-Hohenberg type which supports the formation of cavity solitons, plane waves, and periodic structures. The formation, interaction, and stability of each of the nontrivial spatial structures is considered via extensive numerical simulations. The spectral stability of these nontrivial spatial structures are also investigated using Hill's method. Stable optical structures are created which can be used as the basis for a wide range of all-optical technologies.

*An undergraduate thesis submitted in partial fulfillment of the requirements for an Applied and Computational Mathematical Sciences Honors Degree from the University of Washington.

Contents

1 Introduction **3**

2 The Optical Parametric Oscillator Near Resonance Detuning **4**

3 Derivation of Order Parameter Equation **6**

4 Plane Wave Solutions **9**

5 Localized Solutions: Light Bullets **12**

6 Periodic Solutions **19**

7 Stability of Solutions **26**

8 Conclusions **27**

1 Introduction

Spatio-temporal dynamics in nonlinear systems are of general interest in the physical, biological, and engineering sciences [1]. Specifically, the role of nonlinearity in generating novel applications and technological devices is of ever growing importance. Many media studied in the optical sciences are capable of supporting spatio-temporal electromagnetic structures which are often stabilized by the interaction of spatial diffraction or temporal dispersion with the material nonlinearity. Optical Parametric Oscillators are constructed with quadratic nonlinear materials and are commonly used as tunable sources for coherent radiation [2] and the generation of high power pulses [3]. Parametric mixing between signal and pump fields with cavity diffraction leads to the formation of soliton-like structures referred to as *cavity solitons* or *dissipative solitons*. Such structures, if stabilized, can be used as fundamental components for all-optical devices and applications. Thus, understanding the underlying dynamical aspects of these nontrivial electromagnetic structures is paramount to technological considerations. We consider the formation and stability of two-dimensional electromagnetic structures in an OPO system near the resonance detuning limit. We find a wide variety of exact solutions, including cavity solitons, which are indeed formed and stabilized by the parametric mixing with diffraction.

This manuscript is outlined as follows: Sec. 2 gives a brief background to nonlinear optics and the OPO near resonance detuning. Sec. 3 gives a brief, yet comprehensive, derivation of the governing order parameter equation in the near resonance limit using a multiple-scale analysis. Sec. 4, 5, and 6 consider exact solutions of the plane wave, hyperbolic secant, and periodic Jacobi elliptic forms respectively. The exact solutions are explored and their dynamics and stability investigated. The stability of solutions is explored in Sec. 7. The paper is concluded in Sec. 8 with a brief summary of the paper and comments on possible future work.

2 The Optical Parametric Oscillator Near Resonance Detuning

The invention of the optical laser in the early 1960s made possible the generation of highly intense and coherent electromagnetic radiation. Shortly thereafter, laser light incident on quadratic crystals was observed to induce optical frequency conversion. This founded the field of *nonlinear optics*, which is defined to be the study of the interaction between intense electromagnetic radiation with matter [16].

In conventional optics, the relationship between the electromagnetic field, $E(t)$, and the electric polarization, $P(t)$, is given by a linear relationship, $P(t) = \chi E(t)$, where χ is determined by physical properties of the (linear) medium (known as the linear susceptibility). However, if the intensity of the light is sufficiently large, light interacts with the medium resulting in a changing polarization [17]. The mediums of interest in this manuscript are those with a nonlinear polarization dominated by the second-order nonlinearity which are called *quadratic materials*.

In an *Optical Parametric Oscillator (OPO)*, a quadratic material is placed inside an optical resonator, a device composed of highly reflective mirrors at either end of an optical cavity. These mirrors force the field, generated by the second-order polarization, to repeatedly pass through the quadratic material. The incident pump beam at frequency ω_p produces two fields: the signal field and the idler field. The frequencies of these fields are related by the equation

$$\omega_p = \omega_s + \omega_i \tag{1}$$

where ω_s is the frequency of the signal field and ω_i is the frequency of the idler field. The advantage of this configuration is the frequency of the signal field (which is the desired field) can be tuned to any value less than the frequency of the pump field [18]. This causes parametric devices to have tuning ranges and efficiency unmatched by conventional laser sources. OPOs should be able to generate radiation throughout interesting spectral regions where conventional devices have failed. Despite the potential, the realization of these devices has been difficult because the fundamental physics describing

the system is not thoroughly understood. Thus, researchers have had a difficult time tuning and stabilizing the OPO. Recent advances in both laser sources and nonlinear-optical materials have increased interest in OPOs with promise of high efficiency and extended operating parameters. Thus rapid progress in optical parametric research has been made recently in theoretical studies and modeling.

The nondimensional parametric interaction of the signal and pump fields in the two-dimensional, degenerate optical parametric oscillator subject to diffraction, attenuation, and external pumping is given by [4, 5]

$$\frac{\partial U}{\partial t} = \frac{i}{2}\nabla^2 U + VU^* - (1 + i\Delta_1)U \tag{2a}$$

$$\frac{\partial V}{\partial t} = \frac{i}{2}\rho\nabla^2 V - U^2 - (\alpha + i\Delta_2)V + S \tag{2b}$$

where $U(x, y, t)$ is the envelope of the signal field at frequency ω, $V(x, y, t)$ is the envelope of the incident pump field at frequency 2ω, and $\nabla^2 = \partial_x^2 + \partial_y^2$. The system is pumped externally by the field $S(x, y, t)$. The parameter ρ measures the diffraction ratio between signal and pump fields while α determines the pump-to-signal loss ratio. Detuning between the signal and pump fields is measured by the parameters Δ_1 and Δ_2. The only known analytic solutions to (2) are plane wave solutions [4] for which stability can be determined explicitly. Although they are of general interest, the stabilization of nontrivial spatial structure is the technologically relevant issue to be considered here. Towards this aim, a variety of asymptotic and perturbation methods have been developed to provide an analytic framework for understanding the dynamics and formation of transverse spatial structures.

To characterize the dynamics of the OPO in a spatially extended system, it is typical to derive an *order parameter equation* which governs the onset of instability [1]. Such analytic methods have been applied extensively to OPOs due to the underlying complexity of the governing evolution equations (2). The simplified order parameter descriptions, given by Ginzburg-Landau or Swift-Hohenberg equations, allow for significant analytic simplification and insight into the physical mechanisms responsible for generating the patterns and dynamics observed in simulations of the full governing OPO equations. The literature describing such analytic and computational approximations is

vast, but see, for instance, references [6]-[11] as particular examples of pattern forming behavior in the OPO. Often, exact solutions can also be found within the framework of these approximations which are amenable to linear stability analysis, thus allowing for characterization of the dynamical properties of the solutions. Indeed, the prolific use of such approximations attest to the importance and capability of such methods in producing physically meaningful insight into the dynamics of the OPO.

We derive an order parameter equation of the OPO system in the resonantly detuned limit: $|\Delta_2| \ll 1$ and $|\Delta_1| \ll 1$. Specifically, we consider the onset of instability which occurs for the trivial steady-state signal field solution

$$U = 0 \tag{3a}$$

$$V = \frac{S}{\alpha + i\Delta_2}\,. \tag{3b}$$

It is well-known that this solution is unstable when a critical amount of pumping is applied. The resulting spatial structures which arise after bifurcation is the focus of this paper. Specifically, the long-wavelength instability generates a new, order parameter description similar to the Swift-Hohenberg equation. Analytic solutions to this equation in one-dimension have been studied extensively [12]. Here, the equation is explored in two-dimensions with particular emphasis given to the construction of exact analytic solutions and their stability.

3 Derivation of Order Parameter Equation

We consider the stability of the solution (3) to (OPOeq) with a slight perurbation to the solution:

$$U = 0 + \tilde{u} \tag{4a}$$

$$V = \frac{S}{\alpha + i\Delta_2} + \tilde{v}. \tag{4b}$$

where $\tilde{u}$ and $\tilde{v} \ll 1$. Inserting this into (3) gives the first order equations:

$$\tilde{u}_t = \frac{i}{2}\nabla^2\tilde{u} + \frac{S}{\alpha + i\Delta_2}\tilde{u} - (1 + i\Delta_1)\tilde{u} \tag{5a}$$

$$\tilde{v}_t = \frac{i}{2}\rho\nabla^2\tilde{v} - (\alpha + i\Delta_2)\tilde{u}. \tag{5b}$$

Then denoting the Fourier Transform of $\tilde{u}$ in both the x and y variables as $\hat{u}$ and taking the Fourier Transform of (5) yields:

$$\hat{u}_t = -\frac{i}{2}(k_x^2 + k_y^2)\hat{u} + \frac{S}{\alpha + i\Delta_2}\hat{u} - (1 + i\Delta_1)\hat{u} \tag{6a}$$

$$\hat{v}_t = -\frac{i}{2}\rho(k_x^2 + k_y^2)\hat{v} - (\alpha + i\Delta_2)\hat{u} \tag{6b}$$

where k_x and k_y are the wavenumbers in the x and y directions respectively. From (6) we can see that the the most unstable wavenumbers are $(k_x, k_y) = (0, 0)$. Thus, neutral stability of the steady-state solution (3) occurs when $S_c = (\alpha + i\Delta_2)(1 + i\Delta_1)$. When $|S| > |S_c|$, the steady-state solution is unstable. Furthermore, the instability is a long-wavelength instability since the dominant growth mode corresponds to the zero wavenumber. This suggests the use of a multiple scale expansion to describe the long transverse lengthscales involved in the instability. Additionally, a slow-time scale is required to capture the growth near the bifurcation point. This suggests defining the slow spatial and temporal scales [12]

$$T = \epsilon^4 t \tag{7a}$$

$$\xi = \epsilon x \tag{7b}$$

$$\zeta = \epsilon y \tag{7c}$$

where $\epsilon^2 = |S - S_c| \ll 1$. These slow scales are specifically defined to capture the resonance detuning limit, i.e. $|\Delta_1| \ll 1$ and $|\Delta_2| \ll 1$. When not near resonance detuing, it is appropriate to define different slow scales which, for instance, lead to the Ginzburg-Landau equation or a cubic-quintic diffusion

equation [12]. Other scale balances exist as well which are largely covered in the existing literature [6]-[11].

The order parameter equation is derived by expanding about the steady-state solution (3)

$$U = 0 + \epsilon u(T, \xi, \zeta) \tag{8a}$$

$$V = \frac{S}{\alpha + i\Delta_2} + \epsilon^2 v(T, \xi, \zeta) \tag{8b}$$

where $S - S_c = \epsilon^2 c$ and c is a (complex) constant. This assumes that the solution is within $O(\epsilon^2)$ of the bifurcation point.

Substituting (8) into (2) yields the asymptotic expressions

$$(1 + i\Delta_1)(u - u^*) = \epsilon^2 \left(\frac{i}{2} u_{\xi\xi} + \frac{i}{2} u_{\zeta\zeta} + v u^* + \frac{c u^*}{\alpha + i\Delta_2} \right) + \epsilon^4 u_T \tag{9a}$$

$$(\alpha + i\Delta_2) v = -u^2 + \frac{i}{2} \rho \epsilon^2 \left(v_{\zeta\zeta} + v_{\xi\xi} \right) - \epsilon^4 v_T \,. \tag{9b}$$

This exact expression is now simplified through various asymptotically valid approximations. Specifically, a recursion method is used. Thus, from (9a) we solve for u^* on the left hand side of the equation as a function of ϵ. From (9b) we solve the left hand side of the equation for v as a function of ϵ. These expressions can be substituted back into (9) to derive a new asymptotically valid expression for (9a). Applying solvability conditions (Fredholm-Alternative theorem [13]) results in the compatability equation

$$u_\tau + \frac{1}{4}(\nabla^2 - \omega)^2 u - \gamma u - \sigma u^3 + u^5 + 3\delta u(\nabla u \cdot \nabla u) + 2\delta u^2 \nabla^2 u + O(\epsilon) = 0 \tag{10}$$

where $u = u(\tau, X, Y)$ is now a function of the scaled variables $X = \xi/\sqrt{|\Delta_2|}$, $Y = \zeta/\sqrt{|\Delta_2|}$, and $\tau = T/(2\sqrt{|\Delta_2|})$. The Laplacian $\nabla^2 = \partial_X^2 + \partial_Y^2$ and we define $\sigma = -2\beta$, $\omega = |\Delta_2|\Delta_1/(2\epsilon^2)$, $\gamma = 2\beta c + c^2 + \omega^2/4$, where $\beta = (\alpha - \Delta_1\Delta_2)/\epsilon^2$ and $\delta = \pm 1$ is the sign of Δ_2. This is a two-dimensional generalization of the equation presented in reference [12]. It should be noted that the three-dimensional governing equation for $u = u(\tau, X, Y, Z)$ is equivalent to (10) except clearly the Laplacian is read $\nabla^2 = \partial_X^2 + \partial_Y^2 + \partial_Z^2$.

4 Plane Wave Solutions

The simplest form of solutions to consider are plane waves. In the one-dimensional case, plane wave solutions of (2) can be found and their stability determined [4]. Indeed, these are the only exact solutions known for constant external pumping $S(x, y, t)$. A modulated external pumping can generate a broader class of exact solutions which take the form of fronts, pulses, and periodic wavetrains [12]. The generation of such solutions requires accurate control of the external pumping $S(x, y, t)$ and are thus not considered here.

Plane wave solutions are found by letting

$$u(\tau, X, Y) = A\,. \tag{11}$$

Inserting (11) into (10) gives $A^5 - \sigma A^3 + (\omega^2/4 - \gamma)A = 0$. The quintic equation for A results in five solution branches given by

$$A = \left\{ 0, \sqrt{\frac{\sigma \pm \sqrt{\sigma^2 - \omega^2 + 4\gamma}}{2}}, -\sqrt{\frac{\sigma \pm \sqrt{\sigma^2 - \omega^2 + 4\gamma}}{2}} \right\}\,. \tag{12}$$

Figure 1 depicts the solutions branches as a function of the bifurcation parameter γ.

The linear stability of the plane wave solutions can be determined by peturbing the plane wave about one of the five solution branches:

$$u(\tau, X, Y) = A + \tilde{u}(\tau, X, Y) \tag{13}$$

where $\tilde{u} \ll 1$. The resulting linear evolution equation for $\tilde{u}$ is

$$\tilde{u}_\tau + \frac{1}{4}(\nabla^2 - \omega)^2\tilde{u} - \gamma\tilde{u} - 3\sigma A^2\tilde{u} + 5A^4\tilde{u} + 2\delta A^2\nabla^2\tilde{u} = 0\,. \tag{14}$$

The spectral stability is then determined by Fourier transforming (14) in both X and Y. The resulting differential equation for the spatial wavenumbers is given by

$$\hat{u}_\tau = \left[-\frac{1}{4}k_r^4 - \left(\frac{\omega}{2} - 2\delta A^2\right) k_r^2 - \left(\frac{\omega^2}{4} - \gamma - 3\sigma A^2 + 5A^4\right) \right] \hat{u} \equiv \mathcal{F}(k_r)\hat{u}\,, \tag{15}$$

where $\hat{u}$ is the two-dimensional Fourier transform, and $k_r^2 = k_X^2 + k_Y^2$ is the wavenumber in radial coordinates where k_x and k_y are the wavenumbers in the X and Y direction respectively.

Stability of the plane waves is determined by the sign of $\mathcal{F}(k_r)$. Specifically, for $\mathcal{F}(k_r) > 0$ for any k_r, the solution is unstable. Stability is achieved for $\mathcal{F}(k_r) < 0$ for all values of k_r. Note that $\mathcal{F}(k_r)$ depends upon the parameters γ, σ, ω and δ. Of practical interest is the maximum value of $\mathcal{F}(k_r)$. For unstable solutions, this determines the dominant growth rate of a given instability. This maximum can be determined from $d\mathcal{F}(k_r)/dk_r = 0$ so that

$$k_r \left[k_r^2 - (4\delta A^2 - \omega)\right] = 0\,. \tag{16}$$

The extremal values occur then at $k_r^* = 0$ or $k_r^* = \pm\sqrt{4\delta A^2 - \omega}$. For k_r^* to have values which are nonzero, $4\delta A^2 > \omega$. Thus only three values of k_r^* need to be considered in determining the stability of the five branches of solutions. The growth rate at $k_r^* = 0$ is given by

$$\mathcal{F}(k_r^*) = \mathcal{F}(0) = -\left(\frac{\omega^2}{4} - \gamma - 3\sigma A^2 + 5A^4\right)\,. \tag{17}$$

Likewise, the growth rate for both nonzero k_r is

$$\mathcal{F}(k_r^*) = \mathcal{F}(\pm\sqrt{4\delta A^2 - \omega}) = \gamma + (3\sigma - 2\delta\omega)A^2 - A^4\,. \tag{18}$$

For a specific branch of solution (12), the growth rate and stability properties can be calculated. For instance, consideration of the $A = 0$ branch of solution results in instability for $\gamma > \omega^2/4$ when $\omega > 0$ and instability for $\gamma > 0$ when $\omega < 0$ (see Fig. 1(C) and (D)).

Although this provides a general analytic framework to determine stability, the dependence of (12) and (15) on the sign and value of the three parameters $(\gamma, \sigma, \omega, \delta)$ prevents a simple overall description. Therefore, the remainder of this section limits the parameter space by considering the specific case of $\sigma = \omega = 1$. The stability is then determined as a function of the bifurcation parameter γ for $\delta = \pm 1$. Figure 1 summarizes these results. For $\delta = 1$, all nonzero solutions are unstable. The zero solution itself is stable for $\gamma \in (-\infty, 1/4)$. Note that for $|A| > 1/2$, it can be explicitly found that (18) gives the maximal growth rate of $\mathcal{F}(k_r^*) = 1/4$ (see Fig. 1(A)). For $|A| < 1/2$, the zero mode (17) dominates the instability (see Fig. 1(B)). In contrast, the

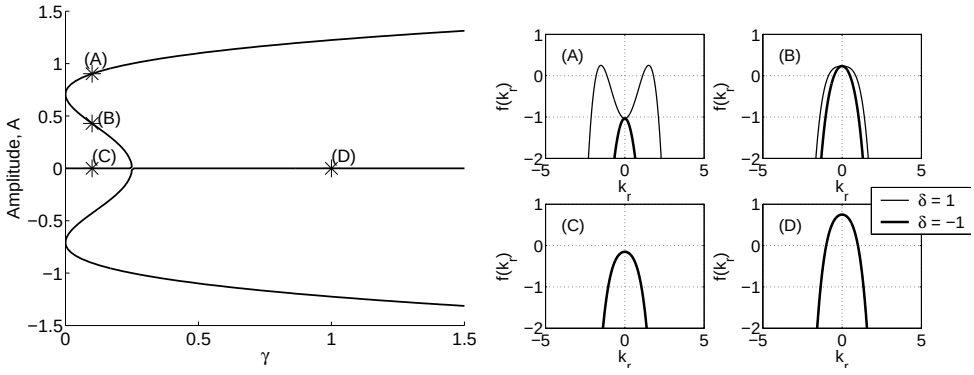

Figure 1: The left hand figure shows the branches of plane wave solutions (12) as a function of the bifurcation parameter γ for $\sigma = \omega = 1$. The right hand figure shows $\mathcal{F}(k_r)$ for $\delta = \pm 1$ for various values along the branches of solutions: (A), (B), (C), and (D). For point (A), the largest growth mode results in a modulational instability (18) for $\delta = 1$. The remaining curves $\mathcal{F}(k_r)$ have a maximum at $k_r = 0$ as given by (17). For (B) and (D), this leads to a long-wavelength instability whereas solutions are stable along (C).

$\delta = -1$ case gives (17) as the maximal growth rate. This is now stable for the top branch of solutions (see Fig. 1(A)). Instability of the middle branch remains unchanged (see Fig. 1(B)).

To further illustrate the dynamial behavior, (10) is numerically integrated. Figure 2 demonstrates the convergence of a wide range of plane wave solutions to the stable top branch or zero branch of solutions for $\delta = -1$. Convergence to the exact solution is rapid with the convergence rate determined from the value of $\mathcal{F}(0)$. The stable two-dimensional evolution is shown in Fig. 3. Note the rapid convergence to the final value of $A = 0.97$ when using $\gamma = 0.2$. The instability of the $\delta = 1$ case is demonstatred in Fig. 4 for $\gamma = 0.2$. Note the onset of a modulational instability which is consistent with the analytic prediction of (18) being the dominant growth mode.

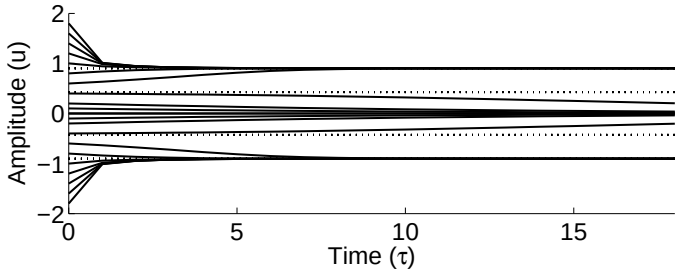

Figure 2: Two-dimensional numerical simulations which confirm that various initial plane waves converge to the analytically predicted values of Fig. 1. For the specific values considered, $\delta = -1$, $\sigma = \omega = 1$, and $\gamma = .2$, the initial conditions converge to $A = \pm .97$ or $A = 0$.

5 Localized Solutions: Light Bullets

One of the fundamentally important solutions to any nonlinear optical system is localized solutions. Indeed, the stabilization of such structures is of paramount importance from an applications standpoint. Often such localized solutions act as the *optical bits* and are the building blocks for all-optical signal processing and switching applications. In two-dimensions, exact solutions of this form are rarely found. However, the evolution equation (10) admits such solutions for $\delta = 1$. Their construction is accomplished by assuming the steady-state form

$$u(\tau, X, Y) = A\,\mathrm{sech}(BX)\,\mathrm{sech}(BY)\,. \tag{19}$$

Inserting (19) into (10) gives for $\delta = 1$

$$A^2 = B^2 \quad \text{or} \quad A^2 = 6B^2 \tag{20a}$$

$$\omega = \pm 2\sqrt{\gamma - B^4} \tag{20b}$$

$$\sigma = (B^2/A^2)\left(\omega - 4B^2 + 3A^2\right)\,. \tag{20c}$$

Cynlindrical symmetry is the key aspect of generating such solutions. The bifurcation parameter in this case is chosen to be γ [12]. Thus given values of γ and B, the remaining parameters are fixed.

In one-dimension, the paramter γ controls the level of linear growth and generates instabilities for $\gamma > 1/4$. Stable solutions only exist in the parameter

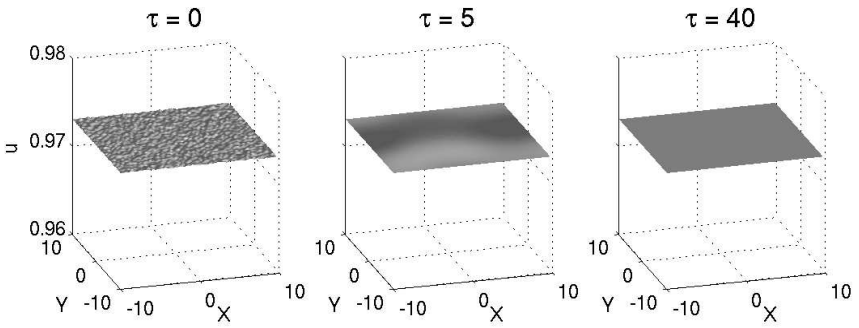

Figure 3: Evolution of two-dimensional plane wave with added white-noise for $\delta = -1$ and $\gamma = 0.2$. The noise is quickly attenuated as the solution converges to its analytic steady-state solution (12). Here $\sigma = \omega = 1$ so that the stable steady-state branch is depicted in Fig. 1(A).

regime $\gamma \in [0, 1/4)$. Likewise, the only stable solutions of the form (19) are found for γ in a small range near zero. The precise value of γ for which the solution destabilizes can be calculated through numerical simulations or a numerical linear stability analysis. Figure 5 shows the evolution of initial conditions which settle to the analytically predicted solutions (19) and (20). In Fig. 5, the initial condition is the exact solution on the branch $A^2 = 6B^2$ with a small amount of initial white-noise and with $\gamma = 0.1$ and $B = 0.25$. The white-noise immediately is attenuated and the evolution remains on the exact solution, indicating stability. The stability of this branch of solutions can be more clearly seen in Fig. 6 where a variety of initial A values are considered for initial conditions of the form (19). The resulting maximum amplitude is plotted as a function of τ and shows the distinct convergence of initial data to the $A^2 = 6B^2$ branch of solutions for sufficiently high values of A. For $|A| < 0.3$, the solutions are attenuated to zero whereas for $|A| > 0.7$ the the two-dimensional light bullets are destabilized.

A variety of interesting phenomena can occur if the solution (19) is destabilized. The parameter space for inducing instability is large and depends upon the values of γ, ω, A, B and σ chosen. In this large parameter space, we fix our parameters and typically vary the value of γ, i.e. as in the one-dimensional case, γ is our bifurcation parameter. But as demonstrated in the preceding paragraph, the initial amplitude can destabilize the solution above

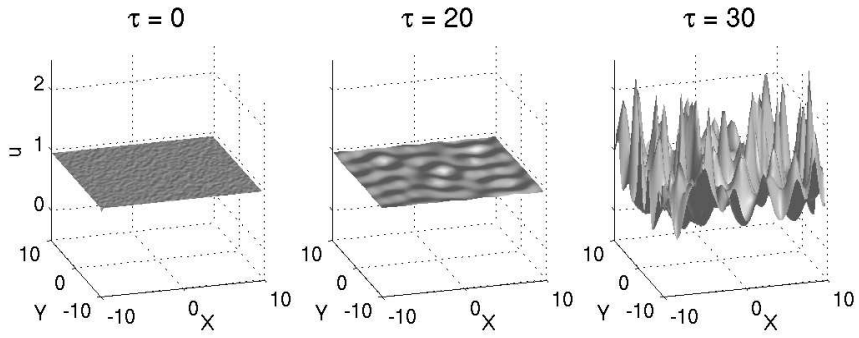

Figure 4: Evolution of two-dimensional plane wave with added white-noise for $\delta = 1$ and $\gamma = 0.2$. The noise quickly seeds the modulational instability predicted by (18) and illustrated in Fig. 1(A). Here we take $\sigma = \omega = 1$.

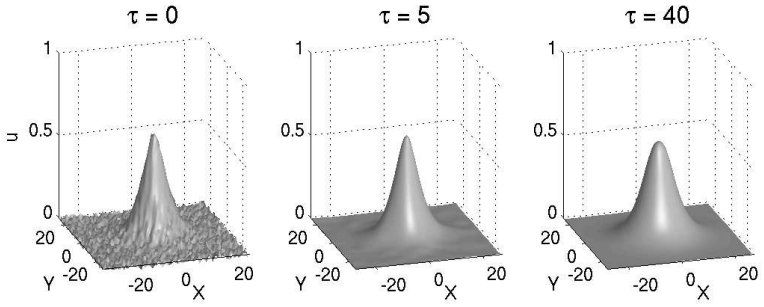

Figure 5: Stable evolution of initial conditions (19) and (20) seeded by white-noise. Here $\gamma = 0.1$ and $B = 0.25$ with $A^2 = 6B^2$.

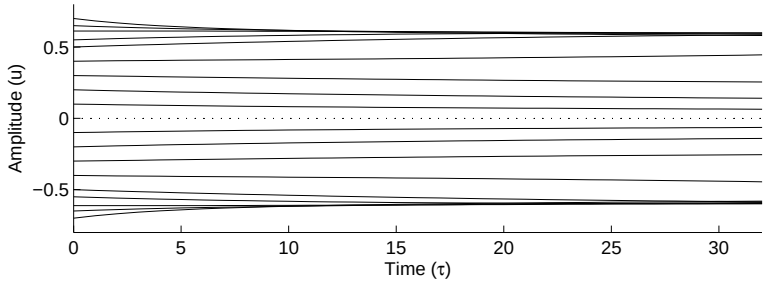

Figure 6: Convergence of initial data given by (19) to stable $A^2 = 6B^2$ solution of Fig. 5. Below $A \approx 0.3$ the trivial solution is an attractor whereas for values of above $A \approx 0.7$, the solution is unstable and evolves to a structure similar to Figs. 7 and 8.

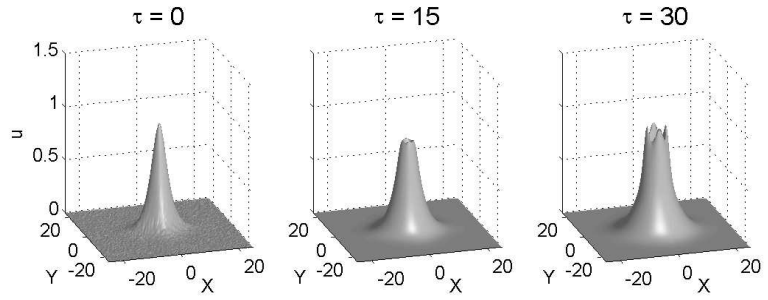

Figure 7: Onset of instability which generates a modulated rim structure on the localized solution. Here we choose $\omega = 0.5$, $A = 1$, and $A^2 = 6B^2$.

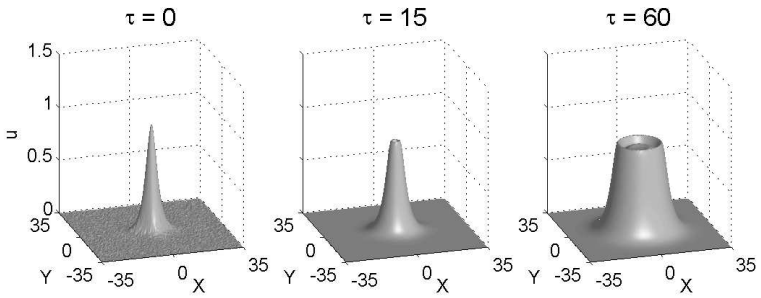

Figure 8: Onset of instability which generates a rim structure on the localized solution which propagates radially outward. Here we choose $\omega = 1$, $A = 1$, and $A^2 = 6B^2$.

a critical threshold value. In Figs. 7-9, the typical instabilities observed in numerical simulations are considered. These simulations represent qualitatively different instability mechanisms which arise from (10) starting with solutions of the type (19). Figure 7 demonstrates the onset of instability which occurs near the peak of the pulse. The pulse peak first flattens and then forms a modulated rim structure which continues to evolve. Figure 8 shows the formation of a localized structure which has a definite rim structure without modulations. In this case, the circular structure continues to expand while keeping the internal amplitude constant. Of greatest interest is Fig. 9 which evolves by first generating concentric rings which evolve into localized, steady-state solutions of alternating signed amplitude. The generation of pulses continues to the boundary at which point a radially-symmetric, quasi-periodic, steady-state pattern is obtained. This stabilization of a collection of localized solutions is further exhibited in Fig. 10 which begins with the initial condition $u(x, y, 0) = \text{sech}(x + y) + \text{sech}(x - y)$ and evolves into a steady-state pattern of localized solutions. The interaction between pulses is critical for stabilizing the configuration.

The stable solutions of the form (19) and demonstrated in Fig. 5 can potentially act as optical bits in technological applications. For all-optical devices, switching and control of such structures is of critical importance. Thus, the pulse-to-pulse interaction between such bits is important to characterize. We consider the interaction of two stable localized bits of the form (19) with (20). For one case, the bits are assumed to be *in-phase* so that the amplitudes are

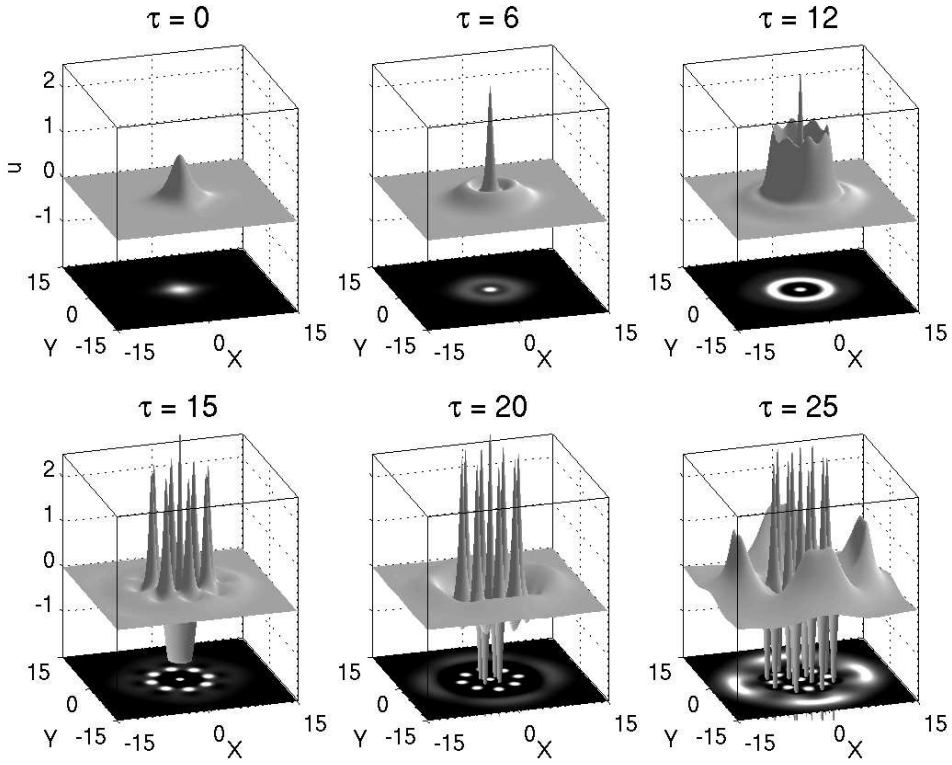

Figure 9: Instability of localized initial condition of the form (19) which evolves by first generating concentric rings which evolve into a pattern of localized, steady-state solutions of the form (19) with alternating signed amplitude. The generation of pulses continues to the boundary at which point a radially-symmetric, quasi-periodic, steady-state pattern is obtained.

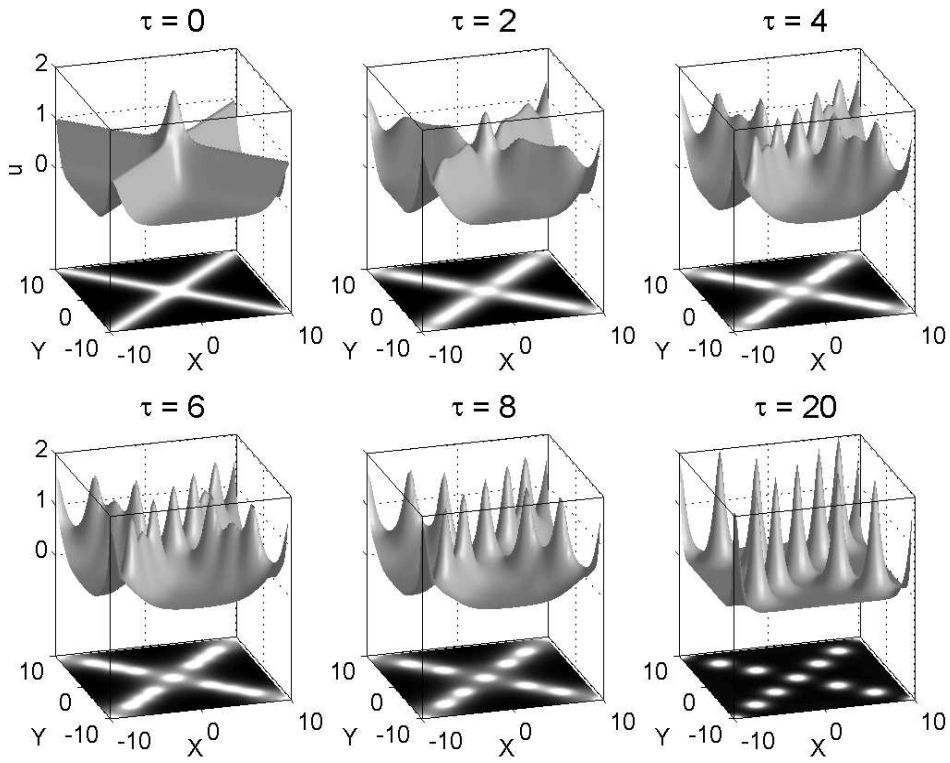

Figure 10: Formation of a stable collection of localized solutions beginning with the initial condition $u(x, y, 0) = \text{sech}(x+y)+\text{sech}(x-y)$. The interaction between pulses is critical for stabilizing the configuration.

both of the same sign. In the second case, the bits are *out-of-phase* so that the amplitudes are of opposite sign. Thus a nodal separation exists between them. The nodal separation is of critical importance for stability considerations [14]. Figures 11 (in-phase) and 12 (out-of-phase) demonstrate the interaction dynamics of the optical bits for these two cases. The in-phase solutions quickly coalesce and form an oblong version of Fig. 8. For long times, the structure evolves into a circularly symmetric shape. In contrast, the out-of-phase solutions are stable, robust, and ideal for applications. For possible logical bit operations, one may be interested in using a control pulse to switch or alter the state of the system. Thus we consider the interaction of three pulses, one of which is of opposite magnitude. The interaction of three pulses evolves towards the canonical two pulse interaction case. Specifically, the two same signed pulses slowly coalesce to form a single pulse much as in Fig. 11. The formation of a new single pulse occurs midway between the pulses. What then remains is a steady state solution exhibited in Fig. 12. Figure 13 exhibits this phenomena for two different configurations. The first configuration (Fig. 13a) begins with the stable configuration of Fig. 12 and perturbs it with a third localized pulse. The configuration destabilizes as the two positive pulses begin to coalesce. The second configuration (Fig. 13b) begins with the unstable configuration of Fig. 11 and perturbs it with a third, opposite signed localized pulse. The configuration again destabilizes as the two positive pulses begin to coalesce. For both of these cases, the coalescence is a slow process which eventually leads back to the stable configuration Fig. 12.

6 Periodic Solutions

The ability of the system (10) to stabilize localized structures is critical for applications. The interaction dynamics between such structures is also of importance for all-optical switching and logic operations. The previous section clearly shows that the system supports stable, interacting localized structures. To generalize this further, we attempt to construct periodic solutions of (10). This is motivated by the large number of periodic solutions found in the one-dimensional case [12]. Candidates for such solutions are the Jacobi elliptic functions [15] which are generalizations of both the hyperbolic functions ($\mathrm{sech}X$ and $\tanh X$) and the sinusoidal functions ($\cos X$ and $\sin X$).

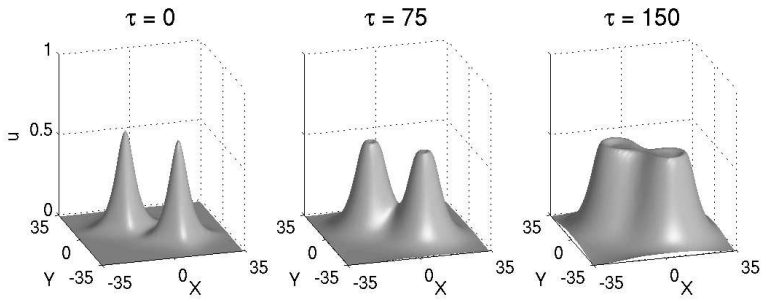

Figure 11: Interaction of two localized solutions (19) of the same sign. Without a nodal separation between them, the pulses are in-phase and are unstable. Specifically, the pulses begin to coalesce into a single localized solution.

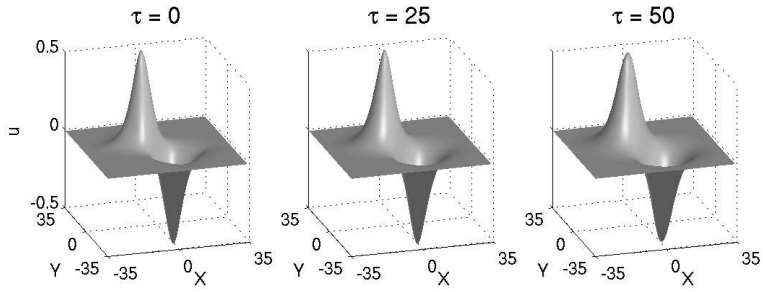

Figure 12: Interaction of two localized solutions (19) of opposite sign. With a nodal separation between them, the pulses are out-of-phase and are stable.

We begin by considering solutions of the form

$$u(\tau, X, Y) = A\mathrm{cn}(BX, k)\mathrm{cn}(BY, k)\,, \tag{21}$$

where k is the elliptic modulus. The Jacobi elliptic $\mathrm{cn}(X, k)$ solution becomes $\cos(X)$ for $k = 0$ and a series of well-separated $\mathrm{sech}X$ solutions of alternating positive and negative amplitudes for $k \to 1$. Plugging (21) into (10) results in a system which cannot be solved exactly. However, along the lines $X = 0$ and $Y = 0$ and with $\delta = 1$, a solution can be found explicitly. Since (21) is periodic in X and Y, this result also holds along lines an integer period distance away from $X = 0$ and $Y = 0$. Thus, we can find an analytic representation of the solutions at every $(X, Y) = (nP, mP)$ where P is the

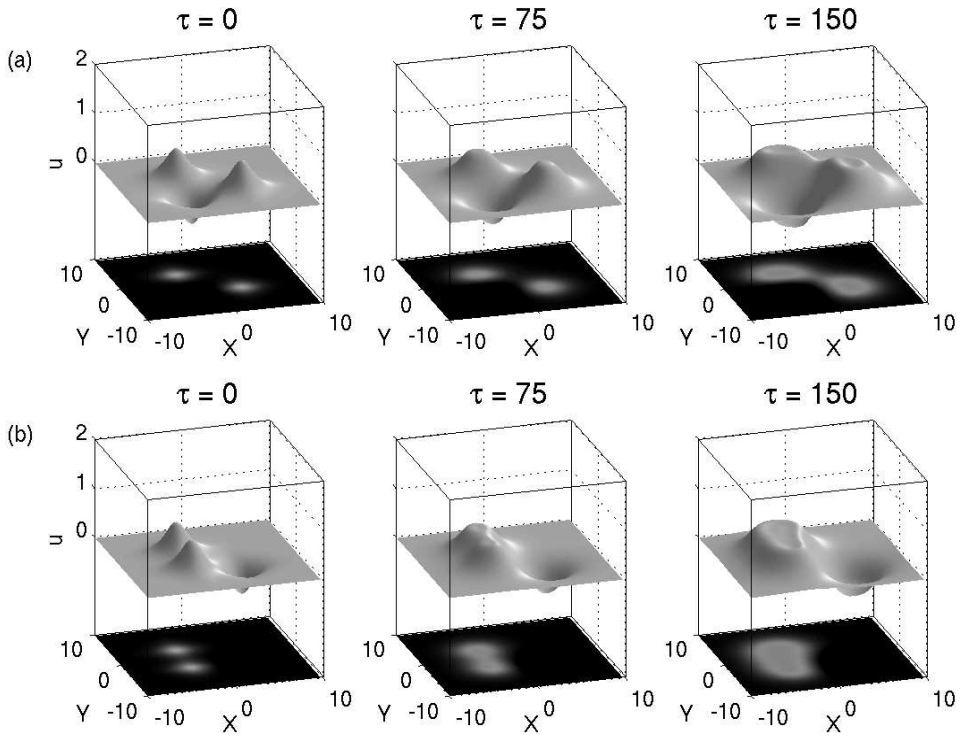

Figure 13: Interaction of three pulses for two different configurations. The first configuration (a) begins with the stable configuration of Fig. 12 perturbed by a third localized pulse. The configuration destabilizes as the two positive pulses begin to coalesce. The second configuration (b) begins with the unstable configuration of Fig. 11 perturbed by a third, opposite sign localized pulse. This configuration also begins to coalesce. For both of these cases, the coalescence is a slow process which eventually leads back to the stable configuration Fig. 12.

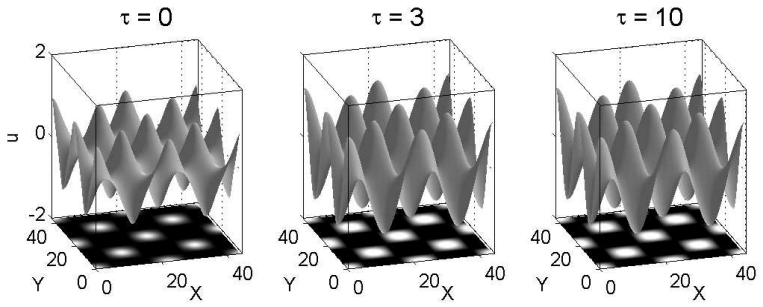

Figure 14: Evolution of (21) with (22) to a steady-state solution with $k = 0.9$, $A = 1$, $\omega = 1$, and starting on the $A^2 = 6B^2$ branch.

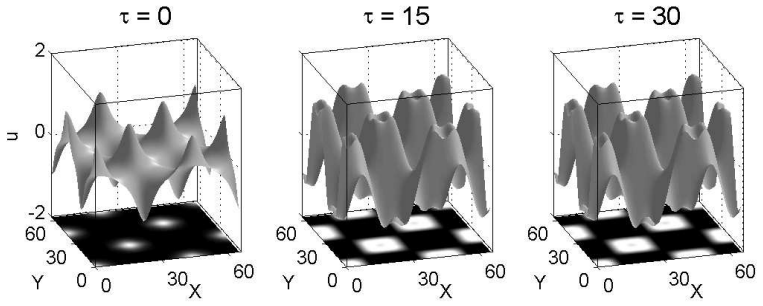

Figure 15: Evolution of (21) with (22) to a steady-state solution with $k = 0.99$, $A = 1$, $\omega = 1$, and starting on the $A^2 = 6B^2$ branch. The higher value of elliptic modulus k, in comparison with Fig. 14, leads to an instability which generates a new steady-state structure with similar features to Figs. 7 and 8.

period of $\mathrm{cn}(BX,k)$ and n, m are integers. Specifically we find

$$\begin{aligned} A^2 &= k^2B^2 \quad \text{or} \quad A^2 = 6k^2B^2 && \text{(22a)}\\ \sigma &= (k^2(6+2k^2)B^4 + 2A^4 - (7+4k^2)A^2B^2 + \omega k^2B^2)/A^2 && \text{(22b)}\\ \gamma &= \omega^2/4 + (1-4k^2-2k^4)B^4 + \omega(1-k^2)B^2 - A^4 + (3+4k^2)A^2B^2 && \text{(22c)} \end{aligned}$$

Although this is not an exact solution for all X and Y, it holds along a periodic lattice. Numerically integrating (10) with the initial condition (21) can quickly settle to a steady-state solution which is perturbatively close to that constructed. Figure 14 demonstrates this evolution. And as with previous localized solutions, (21) can destabilize and form structures observed previously. For instance, Fig. 15 demonstrates a similar structure to that of Fig. 7. The only difference between Figs. 14 and 15 is the value of the elliptic modulus k which is $k = 0.9$ and $k = 0.99$ respectively. Note that even when destabilized the resulting pulse-to-pulse interaction holds the lattice structure together.

We next consider solutions of the form

$$u(\tau, X, Y) = A\mathrm{dn}(BX,k)\mathrm{dn}(BY,k)\,, \tag{23}$$

where again k is the elliptic modulus. The Jacobi elliptic $\mathrm{dn}(X,k)$ solution becomes unity for $k = 0$ and a series of well-separated $\mathrm{sech}X$ solutions of same signed amplitudes for $k \to 1$. Plugging (23) into (10) results in system which cannot be solved exactly. However, as before an analytic representation of the solutions at every lattice point $(X,Y) = (nP, mP)$ can be found. This gives

$$\begin{aligned} A^2 &= B^2 \quad \text{or} \quad A^2 = 6B^2 && \text{(24a)}\\ \sigma &= ((2+6k^2)B^4 + 2A^4 - (7k^2+4)A^2B^2 + \omega B^2)/A^2 && \text{(24b)}\\ \gamma &= \omega^2/4 - (2+4k^2-k^4)B^4 - \omega(1-k^2)B^2 - A^4 + (3k^2+4)A^2B^2 && \text{(24c)} \end{aligned}$$

As before, this is not an exact solution for all X and Y, but it holds along a periodic lattice for $\delta = 1$. Numerically integrating (10) with the initial condition (23) shows the solution decays to the plane wave solutions considered

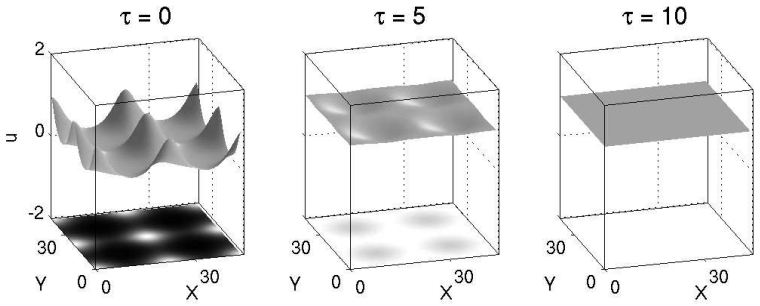

Figure 16: Evolution of (23) with (24) to the steady-state plane wave solution with $k = 0.99$, $A = 1$, $\omega = 1$, and starting on the $A = B$ branch. The decay rate to the plane wave solution is strongly dependent upon the elliptic modulus k, i.e. for $k \to 0$, the decay is much more rapid.

earlier. The decay rate to the plane wave is determined by the elliptic modulus k, i.e. for $k \to 1$ the decay is significantly more rapid than for $k \to 0$. Figure 16 demonstrates the instability of the $\mathrm{dn}(X, k)$ solution.

The remaining Jacobi elliptic function, $\mathrm{sn}(X, k)$, does not allow for the construction of exact solutions along periodic lattice lines as before. The $\mathrm{sn}(X, k)$ solution becomes $\sin X$ for $k = 0$ and a series of well-separated $\tanh X$ front solutions as $k \to 1$. Regardless, we can still numerically integrate (10) with the initial conditions

$$u(\tau, X, Y) = A\mathrm{sn}(BX, k)\mathrm{sn}(BY, k)\,, \tag{25}$$

where A, B, and k are now chosen independently. One choice is to pick these values according to those given by (22) or (24). Figure 17 depicts the convergence of the initial condition (25) with (24) to a steady-state solution. This again demonstrates the stabilizing influence of pulse-to-pulse interactions in the OPO cavity. An example of more complicated steady-state, spatial structure is illustrated in Fig. 18. Regardless, the pulse-to-pulse interaction preserves the stability of the periodic structure.

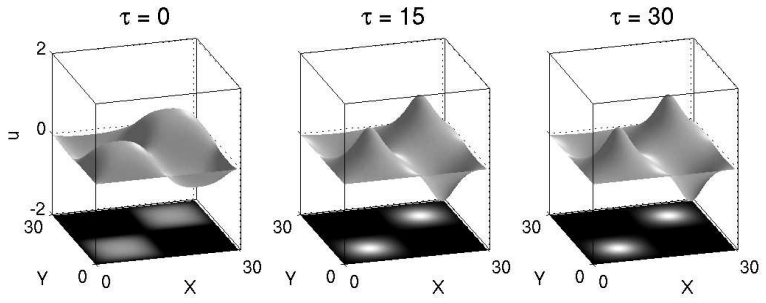

Figure 17: Evolution of (25) using (22) to a steady-state solution with $k = 0.9$, $A = 0.6$, $\omega = 0.5$, and starting on the $A = B$ branch. The solution quickly settles to localized solutions which have nodal separation.

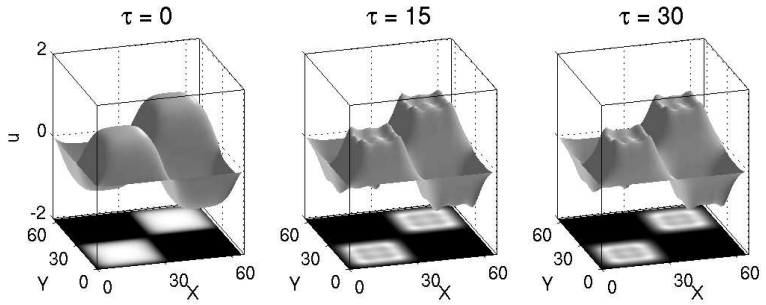

Figure 18: Evolution of (25) using (22) to a steady-state solution with $k = 0.99$, $A = 1$, $\omega = 1$, and starting on the $A^2 = 6B^2$ branch. The solution quickly settles to localized solutions which have nodal separation and nontrivial spatial structure resembling Figs. 7 and 8.

7 Stability of Solutions

Having obtained non-trivial localized solutions to Eq (10), we wish to determine analytically if these solutions are stable. For the plane wave solutions (Sec. 4), it was reasonably easy to analytically determine the stability using a Fourier transform. This is an unreasonable approach for other solutions such as the localized solutions: (19) and (20).

We proceed similarly as in the plane wave case, intuitively asking what is the reaction of the system to a small perturbation of an equilibrium solution? If the perturbed solution returns to the equilibrium solution, than the solution is said to be stable. If the perturbed solution wanders away from the equilibrium solution, than the solution is said to be unstable. Formally, an equilibrium solution $U(x)$ of a dynamical system $\dot{u} = X(u)$ is *spectrally stable* if the spectrum of the linear operator obtained by linearizing $X(u)$ around $U(x)$ has no strictly real part [19].

Linearizing the governing equation (10) about $U(\tau, X, Y) = u(X, Y) + \epsilon v(\tau, X, Y)$ where $u(X, Y)$ is an equilibrium solution gives:

$$v_\tau = \mathcal{L}[u(X,Y)]v + \mathcal{O}(\epsilon) \tag{26}$$

where

$$\mathcal{L} \equiv -\big(\frac{1}{4}(\nabla^2 - \omega)^2 - \gamma - 3\sigma u^2 + u^4 + 3\delta(\nabla u \cdot \nabla u) + 4\delta u \nabla^2 u + 2\delta u^2 \nabla^2 + 6\delta u(u_x \partial_x + u_y \partial_y)\big) \tag{27}$$

Notice that (26), (27) reduce to (14) for the case of constant equilibrium solution: $u(X, Y) = A$. Since the right hand side of (26) is independent of τ, separation of variables

$$v(\tau, X, Y) = w(X, Y)e^{\lambda\tau} \tag{28}$$

results in the leading order eigenvalue problem:

$$\mathcal{L}[u(X,Y)]w(X,Y) = \lambda w(X,Y) \tag{29}$$

From the above definition of spectral stability it is clear that if (29) is satisfied for $Re(\lambda) > 0$ than the solution $u(X, Y)$ is unstable. There are two methods for determining the spectrum of linear operators with periodic coefficients such as $\mathcal{L}[u(X, Y)]$: finite difference methods and the Floquet-Fourier-Hill method [19]. After only partial success at computing the linear spectra using the finite difference method, we implement Hill's method. Hill's method can be used to compute the spectra for linearized operators with periodic coefficients. The advantages of Hill's method over the finite difference method are given in full in [19] but are summarized as follows:

- Hill's method relies on Fourier series and is thus spectrally accurate.
- The use of Floquet theory in Hill's method gives a more uniform approximation of the components of the spectrum rather than isolated elements of it.
- The matrices used in the QR algorithm for the computation of eigenvalues are typically much smaller than for the finite difference methods considerably reducing the time needed to compute spectra.

As a check on our implementation of Hill's method we again consider the stability of the plane wave solutions found in Section 4. Figure 19 gives the approximation via Hill's method to the linearized spectrum expanded about the constant solution (11) for the same parameter values considered in the stability analysis in Fig. 1. It is found that the stability obtained via Hill's method agrees with that found in Fig. 1 obtained using Fourier Transforms.

The implementation of Hill's method to study the stability of localized solutions is sufficiently more complicated that it will not be considered here. However it is clear that this is the method that would be best used to compute the stability of the linearized spectrum expanded about the localized solution of hyperbolic secant form (19) with (20).

8 Conclusions

We have considered the formation and stability of two-dimensional electromagnetic structures in an OPO system near the resonance detuning limit. We found exact solutions for a wide variety of two-dimensional patterns, includ-

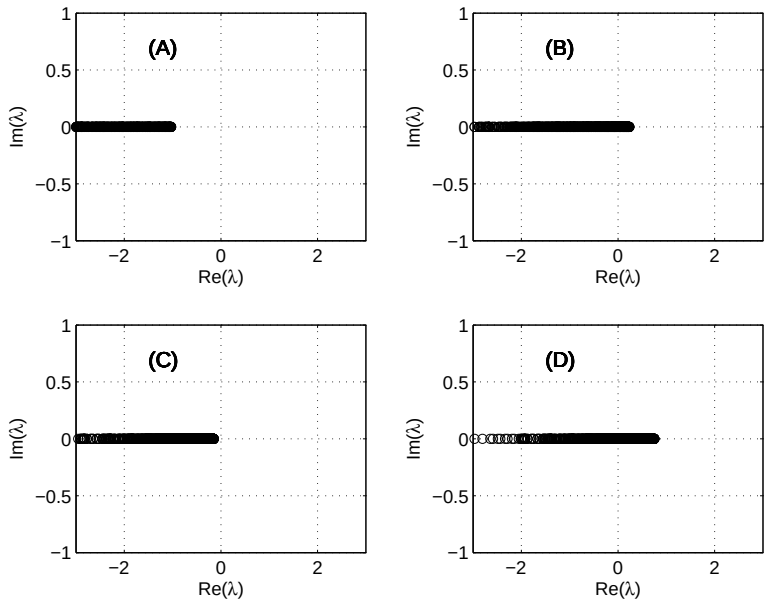

Figure 19: An approximation to the linearized spectrum about the constant solution (11) obtained via Hill's method. The parameter values for the four solutions (A), (B), (C), and (D) correspond to that in Fig. 1 for $\delta = -1$. The stability of each solution agrees with that found in Fig. 1.

ing cavity solitons, which are indeed formed and stabilized by the parametric mixing with diffraction. The stabilization of such structures is of paramount importance from an applications standpoint. Such localized solutions could serve as *optical bits* and their interaction dynamics the building blocks for all-optical signal processing and switching applications. The stabilization of such nontrivial spatial structures was considered via extensive numerical simulations and the framework for analytically examining the spectral stability of these structures using Hill's method was discussed. The work considered here suggests some promising results concerning the possible technological uses of the OPO operating near the resonance detuning limit.

The governing equation (10) considered in this manuscript can be easily extended to three dimensions as briefly discussed in Section 3. Localized solutions similar to the form (19) exist and as in the two-dimensional case, it is probable that these solutions are stable in some parameter regions.

References

[1] M. C. Cross and P. C. Hohenberg, Rev. Mod. Phys. **65**, 851 (1993).

[2] See, for instance, th special issues on Optical Parametric Oscillation and Amplification, J. Opt. Soc. Am. B **10**, 1655-1791 (1993) and Optical Parametric Devices, J. Opt. Soc. Am. B **12**, 2083-2320 (1995).

[3] J. C. Diels and W. Rudulph, *Ultrashort Laser Pulse Phenomena*, (Academic, London, 1996).

[4] S. Trillo, M. Haelterman, and A. Sheppard, "Stable topological spatial solitons in optical parametric oscillators," Opt. Lett. **22**, 970 (1997).

[5] S. Trillo and M. Haelterman, "Excitation and bistability of self-trapped signal beams in optical parametric oscillators," Opt. Lett. **23**, 1514 (1998).

[6] G. L. Oppo, M. Brambilla and L. A. Lugiato, Phys. Rev. A **49**, 2028 (1994).

[7] G. L. Oppo, M. Brambilla, D. Camesasca, and L. A. Lugiato, J. Mod. Opt. **41**, 1151 (1994).

[8] G. J. de Valcárel, K. Staliunas, E. Roldán, and V. J. Sánchez-Morcillo, "Transverse patterns in degenerate optical parametric oscillation and degenerate four-wave mixing," Phys. Rev. A **54**, 1609 (1996).

[9] C. Etrich, D. Michaelis, and F. Lederer, "Bifurcations, stability, and multistability of cavity solitons in parametric downconversion," J. Opt. Soc. Am. B **19**, 792 (2002).

[10] D. V. Skryabin and W. J. Firth, "Interaction of cavity solitons in degenerate optical parametric oscillators," Opt. Lett. **24**, 1056 (1999).

[11] V. J. Sánchez-Morcillo, E. Roldán, and G. J. de Valcárel, and K. Staliunas, "Generalized complex Swift-Hohenberg equation for optical parametric oscillators," Phys. Rev. A **56**, 3237 (1997).

[12] S. Hewitt and J. N. Kutz, *The Optical Parametric Oscillator Near Resonance Detuning*, (submitted) SIAM Journal on Applications of Dynamical Systems.

[13] B. Friedman, *Principles and Techniques of Applied Mathematics*, (Wiley-Interscience, New York, 1991).

[14] J. C. Alexander, M. G. Grillakis, C. K. R. T. Jones, and B. Sandstede, Zeitschrift fr Angewandte Mathematik und Physik **48**, 175 (1997).

[15] M. Abramowitz and I. Stegun, *Handbook of Mathematical Functions*, (Dover, New York, NY 1972).

[16] Optical Parametric Devices, J. Opt. Soc. Am. B **12**, 2083-2320 (1995).

[17] J. Jackson *Classical Electrodynamics*, 1999.

[18] Sarah Hewitt's PhD Thesis. University of Washington. (2004).

[19] B. Deconinck and J. N. Kutz, *Computing spectra of linear operators using Hill's method*, (submitted) Journal of Applied Methods.